SIAM J. SCI. COMPUT.
Vol. 39, No. 5, pp. A1928–A1950

HERMITE SPECTRAL METHODS FOR FRACTIONAL PDEs IN UNBOUNDED DOMAINS*

ZHIPING MAO† AND JIE SHEN‡

Abstract. Numerical approximations of fractional PDEs in unbounded domains are considered in this paper. Since their solutions decay slowly with power laws at infinity, a domain truncation approach is not effective as no transparent boundary condition is available. We develop efficient Hermite-collocation and Hermite–Galerkin methods for solving a class of fractional PDEs in unbounded domains directly, and derive corresponding error estimates. We apply these methods for solving fractional advection-diffusion equations and fractional nonlinear Schrödinger equations.

Key words. fractional PDEs, Hermite polynomials/functions, spectral method, error estimate, unbounded domain

AMS subject classifications. 65N35, 65M70, 41A05, 41A25

DOI. 10.1137/16M1097109

1. Introduction.

Physically motivated space fractional diffusion equations are mostly set in unbounded domains. However, most of the existing numerical approaches are based on domain truncation with ad hoc boundary conditions. While a domain truncation approach can be effective if accurate transparent boundary conditions are available or solutions delay exponentially, it is particularly ineffective for space-fractional PDEs since their solutions decay slowly with power laws at infinity and no transparent boundary condition is available. Furthermore, the domain truncation to fractional derivatives also introduces artificial singularities at the truncated boundary. Therefore, such approaches would not lead to accurate results even with large truncated domains. Due to the lack of accurate transparent boundary conditions, an alternative approach is to solve fractional PDEs on unbounded domains directly. Since spectral methods based on orthogonal functions have proven to be successful for regular PDEs in unbounded domains [5, 19, 17], we aim to construct efficient and accurate spectral methods to solve space-fractional PDEs directly in unbounded domains.

Besides the slow decay at infinity, another major difficulty is the nonlocal feature of fractional derivatives, making it expensive to evaluate the fractional derivatives and to invert the associated system. In the case of bounded rectangular domains, this problem has been well addressed by using the fractopolynomials, introduced in [23]; see also the generalized Jacobi functions (GJFs) in [6]. More precisely, a fractional derivative of fractopolynomials/GJFs is simply another fractopolynomial/GJF with

*Submitted to the journal's Methods and Algorithms for Scientific Computing section October 4, 2016; accepted for publication (in revised form) March 29, 2017; published electronically September 12, 2017.

http://www.siam.org/journals/sisc/39-5/M109710.html

Funding: This work is supported in part by ARO MURI W911NF-15-1-0562, AFOSR FA9550-16-1-0102, NSF DMS-1620262, and NSFC 11371298 and 91630204.

†Division of Applied Mathematics, Brown University, 182 George St, Providence, RI 02912, and Fujian Provincial Key Laboratory on Mathematical Modeling & High Performance Scientific Computing and School of Mathematical Sciences, Xiamen University, Xiamen, Fujian 361005, P. R. China (zhiping_mao@brown.edu).

‡Department of Mathematics, Purdue University, West Lafayette, IN 47907-1957, and Fujian Provincial Key Laboratory on Mathematical Modeling & High Performance Scientific Computing and School of Mathematical Sciences, Xiamen University, Xiamen, Fujian 361005, P. R. China (shen7@purdue.edu).

a different parameter, therefore, fractional derivatives become a local operator in the phase space spanned by fractopolynomials/GJFs. This property led to the very efficient spectral methods for fractional PDEs in bounded domains; see for instance [23, 24, 13, 6]. However, there is no apparent direct extension to fractional PDEs in unbounded domains.

In this paper, we consider a special class of fractional PDEs in an unbounded domain which involves the fractional Laplacian operator $(-\triangle)^{\frac{\alpha}{2}}$ defined through the Fourier transform [15]. While taking the fractional Laplacian under the Fourier transform is a simple and "local" operation, it is, however, very difficult to approximate the (continuous) Fourier transform. Attempts have been made in using the discrete Fourier transform on periodic domains (see, for instance, [11]), but it requires an exceedingly large number of unknowns to achieve a reasonable accuracy. A key observation for our approach is that the Hermite functions are eigenfunctions of the Fourier transform. This fact, together with the definition of the fractional Laplacian through the Fourier transform, makes the fractional Laplacian a local operator in the phase space expanded by Hermite functions. We shall first develop a Hermite-collocation method which is extremely simple to implement, followed by a Hermite–Galerkin method, which is more accurate than the Hermite-collocation method, but still very efficient.

The rest of the paper is organized as follows. In the next section, we provide some preliminaries about Hermite functions and their approximation properties. In section 3, we present the Hermite-collocation method and derive corresponding error estimates. The Hermite-Galerkin method is considered in section 4. In section 5, we present numerical results for model elliptic equations and applications to fractional advection-diffusion equations and fractional nonlinear Schrödinger equations.

2. Preliminaries. We first introduce some definitions and notations which will be used hereafter.

We shall use bold letters such as $\boldsymbol{x} = \boldsymbol{x} = (x_1, \cdots, x_d)$ and $\boldsymbol{j} = (j_1, \cdots, j_d)$ to denote multivariables and multi-indices. For any function $u(\boldsymbol{x}) \in L^2(\Omega)$, we denote its Fourier transform by $\widehat{u}(\boldsymbol{\xi})$. We denote by $|\boldsymbol{\xi}|_1$, $|\boldsymbol{\xi}|_2$, and $|\boldsymbol{\xi}|_\infty$ the l^1, l^2, and l^∞ norm of $\boldsymbol{\xi}$ in $\mathbb{R}^d$, respectively.

DEFINITION 1. *Given $s > 0$, the fractional Laplacian operator $(-\triangle)^s$ is defined by*

$$\widehat{(-\triangle)^s u}(\boldsymbol{\xi}) = |\boldsymbol{\xi}|_2^{2s} \widehat{u}(\boldsymbol{\xi}). \tag{2.1}$$

Let $\omega(\boldsymbol{x}) > 0$ ($\boldsymbol{x} \in \Omega$) be a weight function; we denote by $L^2_\omega(\Omega)$ the usual weighted Hilbert space with the inner product and norm defined by

$$(u, v)_{\Omega,\omega} = \int_\Omega u(\boldsymbol{x}) v(\boldsymbol{x}) \omega(\boldsymbol{x})\, d\boldsymbol{x}, \quad \|u\|_{\Omega,\omega} = (u, u)^{\frac{1}{2}}_{\Omega,\omega} \; \forall\, u, v \in L^2_\omega(\Omega). \tag{2.2}$$

When $\omega \equiv 1$, we will drop ω from the above notations. The Plancherel theorem states that

$$\|u\|_\Omega = \|\widehat{u}\|_\Omega. \tag{2.3}$$

We denote by $H^\mu(\Omega)$ (with $\mu \geq 0$) the usual Hilbert spaces with seminorm

$$|u|_{\mu,\Omega} = \||\boldsymbol{\xi}|_2^\mu \widehat{u}\|_\Omega \tag{2.4}$$

and norm

$$\|u\|_{\mu,\Omega} = (\|u\|^2_\Omega + |u|^2_{\mu,\Omega})^{1/2} = (\|\widehat{u}\|^2_\Omega + \||\boldsymbol{\xi}|_2^\mu \widehat{u}\|^2_\Omega)^{1/2}. \tag{2.5}$$

Let c be a generic positive constant independent of any functions and of any discretization parameters. We use the expression $A \lesssim B$ (resp., $A \gtrsim B$) to mean that $A \leqslant cB$ (resp., $A \geqslant cB$), and use the expression $A \cong B$ to mean that $A \lesssim B \lesssim A$. We will also drop Ω or $\mathbb{R}$ from the notations if no confusion arises.

We recall that the orthonormal Hermite polynomials $\{H_n(x)\}$ are defined by the three-term recurrence relation

$$\begin{aligned} &H_{n+1}(x) = x\sqrt{\frac{2}{n+1}}H_n(x) - \sqrt{\frac{n}{n+1}}H_{n-1}(x),\ n \geq 1, \\ &H_0(x) = \pi^{-1/4}, \quad H_1(x) = \sqrt{2}\pi^{-1/4}x. \end{aligned} \tag{2.6}$$

They are mutually orthogonal with respect to the weight function $\omega(x) = e^{-x^2}$, i.e.,

$$\int_{-\infty}^{\infty} H_m(x)H_n(x)\omega(x)dx = \delta_{mn}, \tag{2.7}$$

and satisfy

$$H_n'(x) = \sqrt{2n}H_{n-1}(x),\ n \geq 1. \tag{2.8}$$

Moreover, $H_n(x)$ is an odd (resp., even) function for n odd (resp., even), that is,

$$H_n(-x) = (-1)^n H_n(x). \tag{2.9}$$

In practice, it is advised to use a problem dependent scaling factor λ to redistribute the Hermite–Gauss collocation points (cf. [21, 17]). We define a sequence of Hermite functions with a scaling parameter λ:

$$\psi_n(x;\lambda) = \sqrt{\lambda}e^{-(\lambda x)^2/2}H_n(\lambda x), \tag{2.10}$$

and denote in particular $\psi_n(x) = \psi_n(x;1)$. It follows from (2.7) that the Hermite functions form an orthonormal basis in $L^2(\mathbb{R})$, i.e.,

$$\int_{-\infty}^{\infty} \psi_m(x;\lambda)\psi_n(x;\lambda)dx = \delta_{mn}. \tag{2.11}$$

We can also derive from (2.6) a three-term recurrence relation for $\psi_m(x;\lambda)$:

$$\begin{aligned} &\psi_{n+1}(x;\lambda) = \lambda x\sqrt{\frac{2}{n+1}}\psi_n(x;\lambda) - \sqrt{\frac{n}{n+1}}\psi_{n-1}(x;\lambda),\ n \geq 1, \\ &\psi_0(x;\lambda) = \sqrt{\lambda}\pi^{-1/4}e^{-(\lambda x)^2/2}, \quad \psi_1(x;\lambda) = \lambda^{\frac{3}{2}}\sqrt{2}\pi^{-1/4}xe^{-(\lambda x)^2/2}. \end{aligned} \tag{2.12}$$

Obviously, $\psi_n(x;\lambda)$ is also an odd (resp., even) function for n odd (resp., even).

The following result (see, for instance, [7, 10]) plays a key role in our algorithm development.

LEMMA 1. *The Hermite function $\psi_n(x), n = 0, 1, \ldots,$ are the eigenfunctions of the Fourier transform operator with eigenvalues $(-\mathrm{i})^n$, $n = 0, 1, \ldots,$ i.e.,*

$$(\widehat{\psi_n(x)})(\xi) = \frac{1}{\sqrt{2\pi}}\int_{-\infty}^{\infty} \psi_n(x;1)e^{-\mathrm{i}\xi x}dx = (-\mathrm{i})^n\psi_n(\xi), \tag{2.13}$$

where $\mathrm{i} = \sqrt{-1}$.

We easily derive from the above and

$$\widehat{(f(ax))}(\xi) = \frac{1}{\sqrt{2\pi}} \int_{-\infty}^{\infty} f(ax) e^{-i\xi x} dx = \frac{1}{|a|} \widehat{f}\left(\frac{\xi}{a}\right) \tag{2.14}$$

the following.

LEMMA 2.

$$\widehat{(\psi_n(x;\lambda))}(\xi) = (-\mathrm{i})^{\mathrm{n}} \psi_{\mathrm{n}}\left(\xi; \frac{1}{\lambda}\right). \tag{2.15}$$

To simplify the presentation, we shall omit the scaling factor λ in the analysis, but we will use different scaling factors in our numerical experiments.

Let P_N be the space of polynomials of degree less than or equal to N, and denote $X_N = \{v : v = e^{-x^2/2} w, \forall\, w \in P_N\}$. Let $\{\eta_j\}_{0\le j\le N}$ be the Hermite–Gauss points, i.e., $H_{N+1}(\eta_j) = 0,\ 0 \le j \le N$, and $\{\omega_j\}_{0\le j\le N}$ be the corresponding weights such that the following Hermite–Gauss quadrature holds [17]:

$$\int_{\mathbb{R}} p(\eta) q(\eta) d\eta = \sum_{j=0}^{N} p(\eta_j) q(\eta_j) \omega_j, \tag{2.16}$$

where $p \cdot q \in X_{2N+1}$. For d-dimensional cases, we set

$$\begin{aligned} &\boldsymbol{j} = (j_1, \cdots, j_d),\ \boldsymbol{\eta_j} = (\eta_{j_1} \cdots, \eta_{j_d}),\ \hat{\boldsymbol{\omega}}_{\boldsymbol{j}} = \Pi_{k=1}^{d} \omega_{j_k}, \\ &\boldsymbol{\psi_j}(\boldsymbol{\eta}) = \Pi_{k=1}^{d} \psi_{j_k}(\eta_k),\ \mathbb{X}_N := X_N^d. \end{aligned}$$

Then, the d-dimensional Hermite–Gauss quadrature reads

$$\int_{\mathbb{R}^d} p(\boldsymbol{\eta}) q(\boldsymbol{\eta}) d\boldsymbol{\eta} = \sum_{|\boldsymbol{j}|_\infty = 0}^{N} p(\boldsymbol{\eta_j}) q(\boldsymbol{\eta_j}) \hat{\boldsymbol{\omega}}_{\boldsymbol{j}}, \tag{2.17}$$

where $p \cdot q \in \mathbb{X}_{2N+1}$. We denote by I_N the Hermite–Gauss interpolation operator from $C(\mathbb{R}^d)$ to $\mathbb{X}_N$ based on the Hermite–Gauss points. We shall use $x_j = \eta_j$ and $\xi_j = \eta_j$ to denote the Hermite–Gauss points in the physical space and phase space, respectively. For the sake of simplicity, we use $\mathbb{X}_N$ to denote the subspaces in both the (real) physical space and (complex) phase space.

2.1. Multivariate Hermite approximations. We denote $\mathbf{1} = \{1, 1, \cdots, 1\} \in \mathbb{N}^d$, and use the following conventions:

$$\boldsymbol{\alpha} \ge \boldsymbol{k} \iff \forall 1 \le j \le d,\ \alpha_j \ge k_j. \tag{2.18}$$

For a given multivariate function $u(\boldsymbol{x})$, we denote the $|\boldsymbol{k}|_1$th (mixed) partial derivative by

$$\partial_{\boldsymbol{x}}^{\boldsymbol{k}} = \frac{\partial^{|\boldsymbol{k}|_1} u}{\partial_{x_1}^{k_1} \cdots \partial_{x_d}^{k_d}} = \partial_{x_1}^{k_1} \cdots \partial_{x_d}^{k_d} u. \tag{2.19}$$

In particular, we denote $\partial_{\boldsymbol{x}}^{s} u := \partial_{\boldsymbol{x}}^{(s,s,\ldots,s)} u$.

Note that, using (2.8) repeatedly, we have

$$\partial_x^k H_n(x) = d_{n,k} H_{n-k}(x),\ n \ge k \ge 0, \tag{2.20}$$

where

$$d_{n,k} = \sqrt{\frac{2^k n!}{(n-k)!}},\ n \geq k \geq 0. \tag{2.21}$$

For the sake of notational convenience, we extend the definition of $d_{n,k}$ to $0 \leq n < k$ by defining

$$d_{n,k} = 0, \quad 0 \leq n < k. \tag{2.22}$$

Equation (2.20) implies that $\{\partial_x^k H_n\}$ are orthogonal with respect to the weighted inner product. More precisely,

$$\|\partial_x^k H_n(x)\|_\omega^2 = h_{n,k} \text{ with } h_{n,k} = d_{n,k}^2, \tag{2.23}$$

where γ_{n-k} is given in (2.7).

Define the d-dimensional tensorial Hermite polynomial and Hermite weight function as

$$\boldsymbol{H_n}(\boldsymbol{x}) = \prod_{j=1}^d H_{n_j}(x_j), \quad \boldsymbol{\omega}(\boldsymbol{x}) = \prod_{j=1}^d \omega(x_j),\ \boldsymbol{x} \in \mathbb{R}^d. \tag{2.24}$$

We derive from (2.20) and (2.23) that

$$\partial_{\boldsymbol{x}}^{\boldsymbol{k}} \boldsymbol{H_n}(\boldsymbol{x}) = \boldsymbol{d_{n,k}} \boldsymbol{H_{n-k}}(\boldsymbol{x}) \text{ with } \boldsymbol{d_{n,k}} = \prod_{j=1}^d d_{n_j,k_j}, \tag{2.25}$$

and

$$\int_{\mathbb{R}^d} \partial_{\boldsymbol{x}}^{\boldsymbol{k}} \boldsymbol{H_n}(\boldsymbol{x}) \partial_{\boldsymbol{x}}^{\boldsymbol{k}} \boldsymbol{H_m}(\boldsymbol{x}) \boldsymbol{\omega}(\boldsymbol{x}) d\boldsymbol{x} = \boldsymbol{h_{n,k}} \boldsymbol{\delta_{nm}}, \tag{2.26}$$

where $\boldsymbol{n}, \boldsymbol{k} \geq 0$, $\boldsymbol{h_{n,k}} = \prod_{j=1}^d h_{n_j,k_j}$, and $\boldsymbol{\delta_{nm}} = \prod_{j=1}^d \delta_{n_j m_j}$.

For $u(\boldsymbol{x}) \in L^2_{\boldsymbol{\omega}}(\mathbb{R}^d)$, we write

$$u(\boldsymbol{x}) = \sum_{\boldsymbol{n} \geq 0} \hat{u}_{\boldsymbol{n}} \boldsymbol{H_n}(\boldsymbol{x}) \text{ with } \hat{u}_{\boldsymbol{n}} = \int_{\mathbb{R}^d} u(\boldsymbol{x}) \boldsymbol{H_n}(\boldsymbol{x}) \boldsymbol{\omega}(\boldsymbol{x}) d\boldsymbol{x}. \tag{2.27}$$

Formally, we have $\partial_{\boldsymbol{x}}^{\boldsymbol{k}} u = \sum_{\boldsymbol{n} \geq \boldsymbol{k}} \hat{u}_{\boldsymbol{n}} \partial_{\boldsymbol{x}}^{\boldsymbol{k}} \boldsymbol{H_n}(\boldsymbol{x})$, and by the orthogonality (2.26), we get

$$\|\partial_{\boldsymbol{x}}^{\boldsymbol{k}} u\|_{\boldsymbol{\omega}}^2 = \sum_{\boldsymbol{n} \geq \boldsymbol{k}} \boldsymbol{h_{n,k}} |\hat{u}_{\boldsymbol{n}}|^2 = \sum_{\boldsymbol{n} \in \mathbb{N}^d} \boldsymbol{h_{n,k}} |\hat{u}_{\boldsymbol{n}}|^2. \tag{2.28}$$

Note that the second equality is a consequence of (2.22).

Let P_N^d be the d-dimensional tensor of P_N. Consider the orthogonal projection $\boldsymbol{\Pi_N} : L^2_{\boldsymbol{\omega}}(\mathbb{R}^d) \to P_N^d$, defined by

$$\int_{\mathbb{R}^d} (\boldsymbol{\Pi}_N u - u) v_N \boldsymbol{\omega}(\boldsymbol{x}) dx = 0 \quad \forall\, v_N \in P_N^d. \tag{2.29}$$

We define the d-dimensional weighted Sobolev spaces

$$B_\omega^m(\mathbb{R}^d) := \left\{ u : \partial_{\boldsymbol{x}}^{\boldsymbol{k}} u \in L^2_{\boldsymbol{\omega}}(\mathbb{R}^d),\ 0 \leq |\boldsymbol{k}|_1 \leq m \right\} \forall m \in \mathbb{N}, \tag{2.30}$$

equipped with the norm and seminorm

$$\|u\|_{B^m_{\boldsymbol{\omega}}(\mathbb{R}^d)} = \Big(\sum_{0\le|\boldsymbol{k}|_1\le m}\|\partial^{\boldsymbol{k}}_{\boldsymbol{x}}u\|^2_{\boldsymbol{\omega}}\Big)^{\frac{1}{2}},\quad |u|_{B^m_{\boldsymbol{\omega}}(\mathbb{R}^d)} = \Big(\sum_{j=1}^d\|\partial^m_{x_j}u\|^2_{\boldsymbol{\omega}}\Big)^{\frac{1}{2}}. \tag{2.31}$$

In particular, we denote $H^m(\mathbb{R}^d) = B^m_{\omega}(\mathbb{R}^d)$ with $\omega = 0$ and $\|\cdot\| = \|\cdot\|_{L^2(\mathbb{R}^d)}$.

The following results are established in [22].[1]

THEOREM 1. *For any $u \in B^m_{\omega}(\mathbb{R}^d)$ and $0 \le l \le m$, we have*

$$\|\boldsymbol{\Pi}_N u - u\|_{B^l_{\omega}(\mathbb{R}^d)} \lesssim N^{(l-m)/2}|u|_{B^m_{\omega}(\mathbb{R}^d)}; \tag{2.32}$$

and if additionally $m \ge d$, we also have

$$\|I_N u - u\|_{B^l_{\omega}(\mathbb{R}^d)} \lesssim N^{d/6+(l-m)/2}|u|_{B^m_{\omega}(\mathbb{R}^d)}. \tag{2.33}$$

Next, we consider approximations by multivariate Hermite functions. Note that for any $u \in L^2(\mathbb{R}^d)$, we have $u\boldsymbol{\omega}^{-1/2} \in L^2_{\boldsymbol{\omega}}(\mathbb{R}^d)$. Define

$$\hat{\boldsymbol{\Pi}}_N u := \boldsymbol{\omega}^{1/2}\boldsymbol{\Pi}_N(u\boldsymbol{\omega}^{-1/2}) \in \mathbb{X}_N. \tag{2.34}$$

Then for $u \in L^2(\mathbb{R}^d)$, we derive immediately from (2.29) that

$$\int_{\mathbb{R}^d}(\hat{\boldsymbol{\Pi}}_N u - u)v_N d\boldsymbol{x} = 0 \quad \forall\, v_N \in \mathbb{X}_N. \tag{2.35}$$

Introduce the operator $\hat{\partial}_{x_j} = \partial_{x_j} + x_j$ which also satisfies

$$\omega^{-1/2}(x_j)\hat{\partial}_{x_j}u(x_j) = \partial_{x_j}\big[\omega^{-1/2}(x_j)u(x_j)\big],$$

and denote $\hat{\partial}_{\boldsymbol{x}} := \prod_{j=1}^d \hat{\partial}_{x_j}$, $\hat{\boldsymbol{\partial}}^{\boldsymbol{k}}_{\boldsymbol{x}} := \prod_{j=1}^d \hat{\partial}^{k_j}_{x_j}$, and define

$$\hat{B}^m(\mathbb{R}^d) := \big\{u : \hat{\partial}^{\boldsymbol{k}}_{\boldsymbol{x}}u \in L^2(\mathbb{R}^d),\ 0 \le |\boldsymbol{k}|_1 \le m\big\}\ \forall m \in \mathbb{N}, \tag{2.36}$$

equipped with the norm and seminorm

$$\|u\|_{\hat{B}^m(\mathbb{R}^d)} = \Big(\sum_{0\le|\boldsymbol{k}|_1\le m}\|\hat{\partial}^{\boldsymbol{k}}_{\boldsymbol{x}}u\|^2\Big)^{\frac{1}{2}},\quad |u|_{\hat{B}^m(\mathbb{R}^d)} = \Big(\sum_{j=1}^d\|\hat{\partial}^m_{x_j}u\|^2\Big)^{\frac{1}{2}}. \tag{2.37}$$

We derive below approximation results for the errors measured in the usual Hilbert space.

THEOREM 2. *For any $u \in \hat{B}^m(\mathbb{R}^d)$ with $m \ge 1$, we have*

$$\|\hat{\boldsymbol{\Pi}}_N u - u\|_{H^{\mu}(\mathbb{R}^d)} \lesssim N^{(\mu-m)/2}|u|_{\hat{B}^m(\mathbb{R}^d)},\quad 0 \le \mu \le m; \tag{2.38}$$

and if additionally $m \ge d$, we also have

$$\|I_N u - u\|_{H^{\mu}(\mathbb{R}^d)} \lesssim N^{d/6+(\mu-m)/2}|u|_{\hat{B}^m(\mathbb{R}^d)},\quad 0 \le \mu \le 1. \tag{2.39}$$

[1] Note that the result proved in [22] was with $d/6$ replaced by $d/3$ in (2.33). It can be improved to $d/6$ by using the improved one-dimensional result in [2].

Proof. We start with the proof of (2.38).

The case $\mu = 0$ is a direct consequence of (2.32) with $l = 0$.

For any $1 \le j \le d$,

$$\partial_{x_j}(\hat{\mathbf{\Pi}}_N u - u) = \boldsymbol{\omega}^{1/2}\partial_{x_j}\big(\mathbf{\Pi}_N(u\boldsymbol{\omega}^{-1/2}) - (u\boldsymbol{\omega}^{-1/2})\big) - x_j\boldsymbol{\omega}^{1/2}\big(\mathbf{\Pi}_N(u\boldsymbol{\omega}^{-1/2}) - (u\boldsymbol{\omega}^{-1/2})\big).$$

We recall (cf. Lemma B.6 in [17]) that

$$\|x_j u\|_{\boldsymbol{\omega}}^2 \le \|u\|_{\boldsymbol{\omega}}^2 + \|\partial_{x_j} u\|_{\boldsymbol{\omega}}^2, \quad 1 \le j \le d,\ \forall u \in H^1(\mathbb{R}^d). \tag{2.40}$$

Therefore, thanks to (2.40), we obtain

$$\begin{aligned}
\|\partial_{x_j}(\hat{\mathbf{\Pi}}_N u - u)\|^2 \le & 2\|\partial_{x_j}\big(\mathbf{\Pi}_N(u\boldsymbol{\omega}^{-1/2}) - (u\boldsymbol{\omega}^{-1/2})\big)\|_{\boldsymbol{\omega}}^2 \\
& + 2\|x_j\big(\mathbf{\Pi}_N(u\boldsymbol{\omega}^{-1/2}) - (u\boldsymbol{\omega}^{-1/2})\big)\|_{\boldsymbol{\omega}}^2 \\
\le & 2\|\mathbf{\Pi}_N(u\boldsymbol{\omega}^{-1/2}) - (u\boldsymbol{\omega}^{-1/2})\|_{\boldsymbol{\omega}}^2 \\
& + 4\|\partial_{x_j}\big(\mathbf{\Pi}_N(u\boldsymbol{\omega}^{-1/2}) - (u\boldsymbol{\omega}^{-1/2})\big)\|_{\boldsymbol{\omega}}^2 \\
\lesssim & N^{1-m}|u\boldsymbol{\omega}^{-1/2}|_{B^m_{\boldsymbol{\omega}}(\mathbb{R}^d)}^2 \lesssim N^{1-m}|u|_{H^m(\mathbb{R}^d)}^2.
\end{aligned}$$

Summing up the above for $1 \le j \le d$, we obtain (2.38) with $\mu = 1$. By recursively applying the above argument, we can prove (2.38) for all positive integer $\mu \le m$. Finally, (2.38) for $0 \le \mu \le m$ can be obtained by a standard space interpolation [1].

Similarly, we can prove (2.39) from (2.33). ∎

2.2. A model problem. In the next two sections, we shall consider, as a model problem, the following fractional PDE:

$$\rho u(\boldsymbol{x}) + (-\triangle)^{\alpha/2} u(\boldsymbol{x}) = f(\boldsymbol{x}) \quad \text{in } \Omega = \mathbb{R}^d; \qquad \lim_{|\boldsymbol{x}|\to\infty} u(\boldsymbol{x}) = 0, \tag{2.41}$$

where $\rho \ge 0$, $\alpha > 0$.

We start by deriving a suitable weak formulation for (2.41).

LEMMA 3. *Let $\mu > 0$, then for any u, $v \in H^\mu(\Omega)$, we have*

$$\big((-\triangle)^\mu u, \overline{v}\big) = \big((-\triangle)^{\frac{\mu}{2}} u, \overline{(-\triangle)^{\frac{\mu}{2}} v}\big), \tag{2.42}$$

where $\overline{v}$ is the complex conjugate of v.

Proof. First, let us recall a useful property of the Fourier transform, namely, for ϕ, $\varphi \in L^2(\Omega)$, we have

$$\int_\Omega \phi\,\overline{\varphi}\,d\boldsymbol{x} = \int_\Omega \widehat{\phi}\,\overline{\widehat{\varphi}}\,d\boldsymbol{\xi}. \tag{2.43}$$

Then

$$\begin{aligned}
\big((-\triangle)^\mu u, \overline{v}\big) = & \big(\widehat{(-\triangle)^\mu u}, \overline{\widehat{v}}\big) = \big(|\boldsymbol{\xi}|_2^{2\mu}\widehat{u}, \overline{\widehat{v}}\big) = \big(|\boldsymbol{\xi}|_2^{\mu}\widehat{u}, \overline{|\boldsymbol{\xi}|_2^{\mu}\widehat{v}}\big) \\
= & \big(\widehat{(-\triangle)^{\frac{\mu}{2}} u}, \overline{\widehat{(-\triangle)^{\frac{\mu}{2}} v}}\big) = \big((-\triangle)^{\frac{\mu}{2}} u, \overline{(-\triangle)^{\frac{\mu}{2}} v}\big).
\end{aligned}$$ ∎

In this paper, we only focus on real-valued functions. To simplify the notation, we denote $s = \frac{\alpha}{2}$, and define

$$A(u, v) = \rho\big(u, v\big) + \big((-\triangle)^{\frac{s}{2}} u, (-\triangle)^{\frac{s}{2}} v\big). \tag{2.44}$$

By the definition in (2.4), we immediately obtain that $A(\cdot,\cdot)$ is continuous and coercive in $H^s(\Omega)\times H^s(\Omega)$.

Then by Lemma 3, a weak formulation for (2.41) is find $u\in H^s(\Omega)$, such that

$$A(u,v)=(f,v)\quad \forall\, v\in H^s(\Omega). \tag{2.45}$$

Thanks to the Lax–Milgram lemma, the above problem admits a unique solution $u\in H^s(\Omega)$ satisfying

$$\|u\|_{H^s}\lesssim \|f\|_{(H^s)'}, \tag{2.46}$$

where $(H^s)'$ is the dual space of H^s.

3. Hermite-collocation method. In this section, we present a Hermite-collocation method for (2.41) and derive corresponding error estimates.

3.1. Formulation of the method. Applying the Fourier transform on both sides of problem (2.41), we derive an equivalent formulation in frequency space:

$$\rho\widehat{u}(\boldsymbol{\xi})+|\boldsymbol{\xi}|_2^{\alpha}\widehat{u}(\boldsymbol{\xi})=\widehat{f}(\boldsymbol{\xi}), \tag{3.1}$$

which implies that

$$\widehat{u}(\boldsymbol{\xi})=\frac{\widehat{f}(\boldsymbol{\xi})}{\rho+|\boldsymbol{\xi}|_2^{\alpha}}. \tag{3.2}$$

Hence, the Fourier transform of the solution can be expressed directly by using the Fourier transform of f. However, we need a numerical procedure to compute an approximation of (continuous) Fourier transforms, and to compute function values in physical space from its approximation of the (continuous) Fourier transform.

We propose the following Hermite-collocation method: Find $u_N\in\mathbb{X}_N$ such that

$$\widehat{u_N}(\boldsymbol{\eta_j})=\frac{\widehat{I_Nf}(\boldsymbol{\eta_j})}{\rho+|\boldsymbol{\eta_j}|_2^{\alpha}}\quad \forall 0\le|\boldsymbol{j}|_1\le N, \tag{3.3}$$

where I_Nf is the interpolation in $\mathbb{X}_N$ of f at the Hermite–Gauss points.

Denoting $\boldsymbol{\psi_n}(\boldsymbol{x})=\Pi_{n=n_1}^{n_d}\psi_n(x_n)$, we describe below the detailed algorithm for (3.3).

Step 1. From the values of $f(\boldsymbol{\eta_j})$ with $0\le|\boldsymbol{j}|_1\le N$, perform a forward discrete Hermite transform to obtain $\tilde{f}_k$ such that

$$I_Nf(\boldsymbol{x})=\sum_{0\le|\boldsymbol{k}|_1\le N}\tilde{f}_{\boldsymbol{k}}\boldsymbol{\psi_k}(\boldsymbol{x}).$$

Step 2. Take the Fourier transform of the above; thanks to (2.13), we obtain

$$\widehat{I_Nf}(\boldsymbol{\xi})=\sum_{0\le|\boldsymbol{k}|_1\le N}\tilde{f}_{\boldsymbol{k}}(-\mathrm{i})^{|\boldsymbol{k}|_1}\boldsymbol{\psi_k}(\boldsymbol{\xi}).$$

Then, compute $\widehat{I_Nf}(\boldsymbol{\eta_j})$ $(0\le|\boldsymbol{j}|_1\le N)$ from the above with a backward discrete Hermite transform.

Step 3. Compute $\widehat{u_N}(\boldsymbol{\eta_j})$ from (3.3), and perform a forward Hermite transform to obtain $\tilde{v}_k$ such that

$$\widehat{u_N}(\boldsymbol{\xi})=\sum_{0\le|\boldsymbol{k}|_1\le N}\tilde{v}_{\boldsymbol{k}}\boldsymbol{\psi_k}(\boldsymbol{\xi}).$$

Step 4. Take the inverse Fourier transform of the above to obtain

$$u_N(\boldsymbol{x}) = \sum_{0\le|\boldsymbol{k}|_1\le N} \tilde{v}_k \mathrm{i}^{|\boldsymbol{k}|_1} \boldsymbol{\psi}_k(\boldsymbol{x}).$$

Finally, we obtain $u_N(\boldsymbol{\eta_j})$ for $0 \le |\boldsymbol{j}|_1 \le N$ from the above by performing a backward Hermite transform.

Remark 1. We observe that the main cost of the above algorithm is one discrete Hermite transform at each step, the cost of which is $O(N^{d+1})$ for the d-dimensional problem.

3.2. Error estimate. By using the exactness of the Hermite–Gauss quadrature, we rewrite the scheme (3.3) in the following variational form:

$$\rho(\widehat{u_N}, \widehat{v}_N) + (|\boldsymbol{\xi}|_2^\alpha \widehat{u_N}, \widehat{v}_N)_N = (\widehat{I_N f}, \widehat{v}_N) \quad \forall \widehat{v}_N \in \mathbb{X}_N, \tag{3.4}$$

where

$$(u, v)_N \equiv \sum_{0\le|\boldsymbol{j}|_\infty\le N} u(\boldsymbol{\eta_j}) v(\boldsymbol{\eta_j}) \hat{\boldsymbol{\omega}}_{\boldsymbol{j}} \tag{3.5}$$

is the multidimensional discrete inner product defined by the Hermite–Gauss quadrature in (2.17).

We also derive from (3.1) that

$$\rho(\widehat{u}, \widehat{v}_N) + (|\boldsymbol{\xi}|_2^\alpha \widehat{u}, \widehat{v}_N)_N = (\widehat{f}, \widehat{v}_N) + (I_N(|\boldsymbol{\xi}|_2^\alpha \widehat{u}) - |\boldsymbol{\xi}|_2^\alpha \widehat{u}, \widehat{v}_N) \quad \forall \widehat{v}_N \in \mathbb{X}_N. \tag{3.6}$$

Let us define the bilinear form

$$a_N(\widehat{u}, \widehat{v}) = \rho(\widehat{u}, \widehat{v}) + (|\boldsymbol{\xi}|_2^\alpha \widehat{u}, \widehat{v})_N \ \forall \widehat{u}, \widehat{v} \in \mathbb{X}_N, \tag{3.7}$$

and the discrete norm

$$\|\widehat{v}\|_{N,\alpha} \equiv \sqrt{a_N(\widehat{v}, \widehat{v})}. \tag{3.8}$$

By definition, we have

$$\|\widehat{v}\|^2 \lesssim a_N(\widehat{v}, \widehat{v}) = \|\widehat{v}\|_{N,\alpha}^2, \quad a_N(\widehat{u}, \widehat{v}) \lesssim \|\widehat{u}\|_{N,\alpha} \|\widehat{v}\|_{N,\alpha}. \tag{3.9}$$

Hence, applying the first Strang lemma [20] to (3.6) and (3.4), we obtain immediately

$$\|\widehat{u} - \widehat{u_N}\|_{N,\alpha} \lesssim \inf_{\widehat{v}_N \in \mathbb{X}_N} \|\widehat{u} - \widehat{v}_N\|_{N,\alpha} + \|\widehat{f} - \widehat{I_N f}\| + \|I_N(|\boldsymbol{\xi}|_2^\alpha \widehat{u}) - |\boldsymbol{\xi}|_2^\alpha \widehat{u}\|. \tag{3.10}$$

Since

$$\inf_{\widehat{v}_N \in \mathbb{X}_N} \|\widehat{u} - \widehat{v}_N\|_{N,\alpha} \le \|\widehat{u} - I_N \widehat{u}\|_{N,\alpha} = \sqrt{\rho} \|\widehat{u} - I_N \widehat{u}\|,$$
$$\|\widehat{f} - \widehat{I_N f}\| = \|f - I_N f\|$$

and

$$\begin{aligned} I_N(|\boldsymbol{\xi}|_2^\alpha \widehat{u}) - |\boldsymbol{\xi}|_2^\alpha \widehat{u} &= I_N(\rho\widehat{u} + |\boldsymbol{\xi}|_2^\alpha \widehat{u}) - (\rho\widehat{u} + |\boldsymbol{\xi}|_2^\alpha \widehat{u}) + \rho(\widehat{u} - I_N \widehat{u}) \\ &= I_N \widehat{f} - \widehat{f} + \rho(\widehat{u} - I_N \widehat{u}), \end{aligned}$$

we derive from the above and the error estimate (2.39) the following.

THEOREM 3. *Let $\widehat{u}$ and $\widehat{u_N}$ be the solutions to* (3.2) *and* (3.3)*, respectively. Assuming that $\widehat{u} \in \hat{B}^{m_1}(\mathbb{R}^d)$, $f \in \hat{B}^{m_2}(\mathbb{R}^d)$, and $\widehat{f} \in \hat{B}^{m_3}(\mathbb{R}^d)$ with $m_1, m_2, m_3 \geq d$, we have*

$$\|u - u_N\| \lesssim \|\widehat{u} - \widehat{u_N}\|_{N,\alpha} \lesssim N^{d/6-m_1/2}|\widehat{u}|_{\hat{B}^{m_1}(\mathbb{R}^d)} + N^{d/6-m_2/2}|f|_{\hat{B}^{m_2}(\mathbb{R}^d)} + N^{d/6-m_3/2}|\widehat{f}|_{\hat{B}^{m_3}(\mathbb{R}^d)}.$$

Remark 2. We are unable to obtain an optimal error estimate in the energy norm $\|\cdot\|_{H^{\alpha/2}}$ due to the unboundedness of the coefficient $|\boldsymbol{\xi}|_2^{\alpha}$.

4. Hermite–Galerkin method. While the Hermite-collocation method presented above is very easy to implement, its error estimate is not quite optimal as the discrete norm in Theorem 3 is only an approximation to the energy norm $\|\cdot\|_{H^{\alpha/2}}$. Below, we present a Hermite–Galerkin method which enjoys optimal error estimates in the energy norm.

4.1. The method and error estimates. The Hermite–Galerkin approximation for (2.45) is find $u_N \in \mathbb{X}_N$ such that

$$A(u_N, v_N) = (I_N f, v_N) \quad \forall\, v_N \in \mathbb{X}_N. \tag{4.1}$$

Since $\mathbb{X}_N \subset H^s(\Omega)$ for any $s \geq 0$, it is clear that the problem (4.1) admits a unique solution. We derive from (2.45) and (4.1) that

$$A(u - u_N, v_N) = (f - I_N f, v_N) \quad \forall\, v_N \in \mathbb{X}_N.$$

We then derive from a standard argument that

$$\|u - u_N\|_{H^s} \lesssim \inf_{v_N \in \mathbb{X}_N} \|u - v_N\|_{H^s} + \|f - I_N f\|. \tag{4.2}$$

Hence, taking $v_N = \hat{\boldsymbol{\Pi}}_{\boldsymbol{N}} u$ in the above and using Theorem 2, we obtain the following result.

THEOREM 4. *Let u and and u_N be the solutions to* (2.45) *and* (4.1) *respectively. Assuming that $u \in B^{\hat{m}_1}(\mathbb{R}^d)$ and $f \in B^{\hat{m}_2}(\mathbb{R}^d)$ with $m_1 \geq s$, $m_2 \geq d$, we have*

$$\|u - u_N\|_{H^s} \lesssim N^{(s-m_1)/2}|u|_{\hat{B}^{m_1}(\mathbb{R}^d)} + N^{d/6-m_2/2}|f|_{\hat{B}^{m_2}(\mathbb{R}^d)}.$$

Remark 3. The error estimate for the Hermite–Galerkin method is better than that for the Hermite-collocation method in the following two aspects: (i) The error estimate in the Galerkin case is in the energy norm while it only implies an estimate in the L^2-norm in the collocation case; (ii) it only depends on the smoothness of u and f, while in the collocation case it depends on the smoothness of $\widehat{u}$, f, and $\widehat{f}$.

Remark 4. Since the usual duality argument cannot be applied to the fractional differential equations due to the lack of a regularity result, it is not clear how to derive an improved error estimate in the L^2 norm.

4.2. Implementation in one dimension. To implement (4.1), we need to compute the mass matrix $M_{kj} = (\phi_j, \phi_k)$ and stiffness matrix $S_{kj} = \big((-\triangle)^{\frac{s}{2}}\phi_j, (-\triangle)^{\frac{s}{2}}\phi_k\big)$, where $\{\phi_k\}$ are the basis functions of $\mathbb{X}_N$.

Begin with the one-dimensional case. Since $\mathbb{X}_N = \text{span}\{\psi_k(x) : 0 \leq k \leq N\}$, we have $M_{kj} = (\psi_j, \psi_k) = \delta_{kj}$, so we only need to compute S_{kj}. By Lemma 3 and (2.13), we have

$$S_{kj} = \big((-\triangle)^{\frac{s}{2}}\psi_j, (-\triangle)^{\frac{s}{2}}\psi_k\big) = (-\mathrm{i})^j \cdot \mathrm{i}^k \int_{-\infty}^{\infty} |\xi|^{\alpha}\psi_j(\xi)\psi_k(\xi)d\xi. \tag{4.3}$$

To simplify the presentation, we denote $S_{kj} := (-\mathrm{i})^j \cdot \mathrm{i}^k s_{kj}$, and will compute s_{kj}. We have from (2.11) that

$$s_{kj} = \int_{-\infty}^{\infty} |\xi|^\alpha \exp(-\xi^2) H_j(\xi) H_k(\xi) d\xi.$$

For $0 \le j, k \le N$, the above integral can be computed by deriving an analytical recurrence formula for the quantities. Let $\{\tilde{H}_j\}_{j=0}^{\infty}$ denote the generalized Hermite polynomial family orthonormal with respect to the weight function $|\xi|^\alpha \exp(-\xi^2)$ satisfying the following three-term recurrence (see [8, Table 1.1, p. 29]):

$$\sqrt{b_{k+1}}\tilde{H}_{k+1}(x) = x\tilde{H}_k(x) + \sqrt{b_k}\tilde{H}_{k-1}(x),\ k \ge 1,$$
$$\tilde{H}_0(x) = 1/\Gamma(\frac{\alpha+1}{2}),\ \tilde{H}_1(x) = x/\Gamma(\frac{\alpha+1}{2}),$$

where $b_k = k/2$ for k is even while $b_k = k/2 + \alpha/2$ for k is odd. Then there are connection coefficients $c_{n,j}$ so that

$$H_n(x) = \sum_{j=0}^{n} c_{n,j}\tilde{H}_j(x).$$

Therefore, there is an explicit recurrence formula that translates these connection coefficients into $c_{n,j}$ (see [14, (12) and Theorem 1]). Collect these coefficients into the $(N+1)\times(N+1)$ matrix C with $(C)_{j,k} = c_{j,k}$ (using 0-based indexing, $0 \le j, k \le N$). Then the desired matrix is $\hat{S} = CC^T$, where $\hat{S} = \{s_{kj}\}_{k,j=0}^{N}$.

4.3. Implementation in multidimensions. In the one-dimensional case, we developed above an efficient algorithm to compute the stiffness matrix. However, in the multidimensional case, the term $|\boldsymbol{\xi}|_2^\alpha = (\xi_1^2 + \cdots + \xi_d^2)^{\frac{\alpha}{2}}$ in (3.1) is nonseparable, making it very expensive to compute the stiffness matrix explicitly and to solve the resulting linear system by a direct method. Hence, we shall use an iterative approach for (4.1) with a suitable separable problem as a preconditioner. To simplify the presentation, we shall only consider the two-dimensional case, although the method can be directly applied to the multidimensional case.

Unlike in the integer PDE case, the multidimensional fractional PDE (2.41) is no longer separable. This can be easily see from its equivalent formulation in frequency space (3.1) which, in the two-dimensional case, can be written as

$$\rho\widehat{u}(\boldsymbol{\xi}) + (|\xi_1|^2 + |\xi_2|^2)^{\alpha/2}\widehat{u}(\boldsymbol{\xi}) = \widehat{f}(\boldsymbol{\xi}), \tag{4.4}$$

whose Hermite–Galerkin approximation, an equivalent formulation to (4.4), is to find $u_N \in \mathbb{X}_N$ such that

$$\rho(\widehat{u_N}, \widehat{v_N}) + ((|\xi_1|^2 + |\xi_2|^2)^{\alpha/2}\widehat{u_N}, \widehat{v_N}) = (\widehat{I_N f}, \widehat{v_N})\ \forall \widehat{v_N} \in \mathbb{X}_N. \tag{4.5}$$

However, it is convenient to use the following separable form

$$\rho\widehat{u}(\boldsymbol{\xi}) + |\xi_1|^\alpha\widehat{u}(\boldsymbol{\xi}) + |\xi_2|^\alpha\widehat{u}(\boldsymbol{\xi}) = \widehat{f}(\boldsymbol{\xi}) \tag{4.6}$$

to build a preconditioner. Indeed, a Hermite–Galerkin method for (4.6) is to find $u_N \in \mathbb{X}_N$ such that

$$\rho(\widehat{u_N}, \widehat{v_N}) + (|\xi_1|^\alpha\widehat{u_N}, \widehat{v_N}) + (|\xi_2|^\alpha\widehat{u_N}, \widehat{v_N}) = (\widehat{I_N f}, \widehat{v_N})\ \forall \widehat{v_N} \in \mathbb{X}_N. \tag{4.7}$$

Letting $u_N = \sum_{k,j=0}^{N} \tilde{u}_{kj}\psi_k(x_1;\lambda)\psi_j(x_2;\lambda) \in \mathbf{X}_N$ be the solution of (4.7), and setting $\bar{U} = (\tilde{u}_{kj})_{0\le k,j\le N}$ and $\bar{F} = (\tilde{f}_{kj})_{0\le k,j\le N}$ with $\tilde{f}_{kj} = (I_N f, \psi_k(x_1;\lambda)\psi_j(x_2;\lambda))$, the problem (4.7) is reduced to

$$\rho\bar{U} + S\bar{U} + \bar{U}S = \bar{F}, \tag{4.8}$$

where S is the one-dimensional stiffness matrix computed above.

Thus, the above linear system can be efficiently solved by using the matrix diagonalization method [12, 9, 18] in a small multiple of N^3 operations (a small multiple of N^{d+1} operations for d-dimensional problems).

The next lemma shows that (4.7) provides an optimal preconditioner for equation (4.5).

LEMMA 4. *For $0 < \alpha \le 2$, we have*

$$d^{\alpha/2-1}\sum_{j=1}^{d}|\xi_j|^\alpha \le \left(\sum_{j=1}^{d}|\xi_j|^2\right)^{\alpha/2} \le \sum_{j=1}^{d}|\xi_j|^\alpha \quad \forall \xi_1,\dots,\xi_d \in \mathbb{R}.$$

For $\alpha > 2$, we have

$$\sum_{j=1}^{d}|\xi_j|^\alpha \le \left(\sum_{j=1}^{d}|\xi_j|^2\right)^{\alpha/2} \le d^{1-2/\alpha}\sum_{j=1}^{d}|\xi_j|^\alpha \quad \forall \xi_1,\dots,\xi_d \in \mathbb{R}.$$

Proof. It is obvious that the result holds for $\alpha = 2$.

Since $f(x) = -x^{\alpha/2}$ is convex for $x > 0$ with $\alpha \in (0,2)$, we have

$$f\left(\frac{\sum_{j=1}^{d}|\xi_j|^2}{d}\right) \le \frac{1}{d}\sum_{j=1}^{d} f(|\xi_j|^2),$$

which implies

$$\left(\sum_{j=1}^{d}|\xi_j|^2\right)^{\alpha/2} \ge d^{\alpha/2-1}\sum_{j=1}^{d}|\xi_j|^\alpha.$$

On the other hand, we have

$$\sum_{j=1}^{d} a_j \le \left(\sum_{j=1}^{d} a_j^\nu\right)^{1/\nu} \qquad \forall\{a_j \ge 0\},\ 0 \le \mu \le 1.$$

Then letting $a_j = |\xi_j|^2$ and $\nu = \alpha/2$ for $\alpha \in (0,2)$ in the above, we obtain

$$\sum_{j=1}^{d}|\xi_j|^2 \le \left(\sum_{j=1}^{d}|\xi_j|^\alpha\right)^{2/\alpha}.$$

We obtain immediately from the above that

$$\left(\sum_{j=1}^{d}|\xi_j|^2\right)^{\alpha/2} \le \sum_{j=1}^{d}|\xi_j|^\alpha.$$

The case with $\alpha > 2$ can be obtained by using a similar argument. ∎

TABLE 1
Number of iterations for solving (4.4).

	# of iteration					
	$\alpha = 1.2$		$\alpha = 1.5$		$\alpha = 1.8$	
N	$\lambda = 1$	$\lambda = 0.7$	$\lambda = 1$	$\lambda = 0.7$	$\lambda = 1$	$\lambda = 0.7$
60	7	8	6	7	5	6
80	7	8	6	7	5	6
100	7	8	6	7	5	6
120	7	8	6	7	5	6
140	7	8	6	7	5	6
160	7	8	6	7	5	6

Let the linear systems for the original Hermite–Galerkin approximation (4.5) and for the preconditioner (4.7) be $A\bar{u} = \bar{f}$ and $B\bar{u} = \bar{f}$, respectively. Then, the above lemma shows that the condition number of $B^{-1}A$ is uniformly bounded. Since the preconditioner system $B\bar{u} = \bar{f}$ can be efficiently solved, and the matrix-vector product $A\bar{u}$ can be efficiently performed in the frequency space, the linear system $A\bar{u} = \bar{f}$ can then be solved efficiently by using the preconditioned conjugate gradient method.

We now present a numerical example to show the effectiveness of this preconditioner. We consider the problem (2.41) with a random function f and let $\rho \equiv 1$. We set the threshold $\epsilon = 10^{-8}$ and list in Table 1 the iteration numbers of the CG method for solving (4.1) with preconditioner (4.6). We observe that the iteration numbers are bounded independent of N.

5. Numerical results and applications.

5.1. Accuracy tests. In the following, we present a few numerical results to test the accuracy and validate our algorithm. In the first three examples, we shall use the Hermite–Galerkin method, and in Example 5, we shall compare the accuracy of the Hermite–Galerkin method and Hermite-collocation method.

Example 1 (problem with exponential decay solution). Let $\rho \equiv 1$, and the exact solution be $u(x) = e^{-x^2}$. Here we take the scaling parameter $\lambda = 1$.

The L^2 and max errors in semilog scale are showed in Figure 1 for $\alpha = 1.2, 1.8$. We observe an exponential convergence as expected.

Example 2 (problem with smooth and exponential decay forcing function). Letting $\rho \equiv 1$, we take $f(x) = e^{-x^2/2}(1 + x)$. Since no exact solution is available, we use the numerical solution with $N = 512$ as the reference solution. We choose $\lambda = 0.4$.

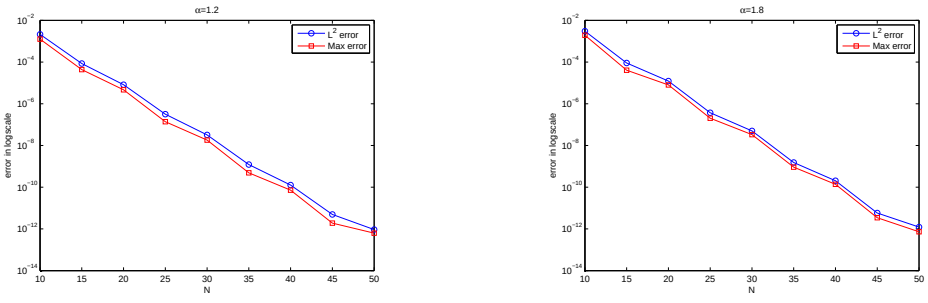

FIG. 1. *Convergence rates for* $u(x) = e^{-x^2}$*; left:* $\alpha = 1.2$*, right:* $\alpha = 1.8$.

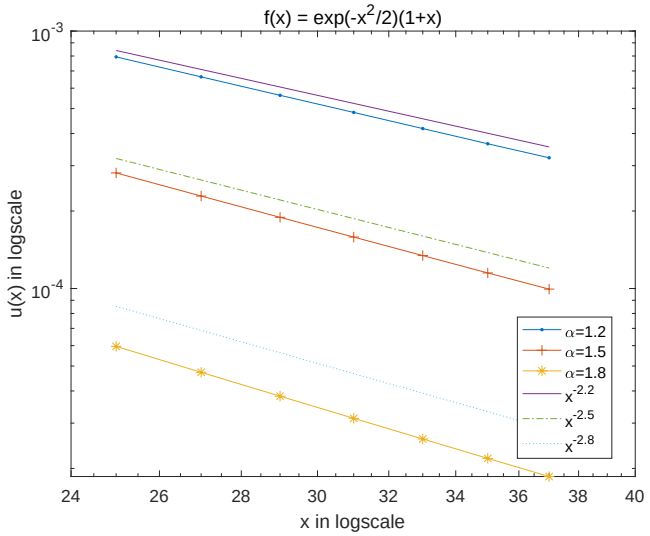

FIG. 2. *Solution* $u(x), x \in (25, 37)$*, for different values of* α *with* $f(x) = e^{-x^2/2}(1 + x)$.

According to Theorem 4, the convergence rate will be essentially depending on the decay rate of the solution at infinity. Hence, we plot in Figure 2 the numerical solution in the interval $x \in (25, 37)$ in log-log scale in order to study the asymptotic behavior of the solution when $|x| \to \infty$. We observe that the solutions have algebraic decay for all noninteger values of α. The asymptotic decay rates for different values of α are also shown in Figure 2, which indicate that the solution behaves like $|x|^{-\alpha-1}$ for large $|x|$. Note that when $\alpha = 2$, the solution does converge exponentially at infinity.

The convergent results in log-log scale are presented in Figure 3. We observe that both L^2-error and $H^{\frac{\alpha}{2}}$-error have algebraic convergence. As expected, the convergence rate improves as α increases. We also list the convergence rates in Tables 2 and 3 for $\alpha = 1.2$ and 1.8, respectively. These numerical results in L^2 indicate a convergence rate of about $\frac{\alpha+1}{2}$, consistent with the decay rate at infinity.

Example 3 (problem with nonexponential decay forcing function). Letting $\rho \equiv 1$, we take $f(x) = \frac{1}{(1+x^2)^2}$. We use the numerical solution with $N = 512$ as the reference solution, and choose $\lambda = 0.7$.

The L^2-error and $H^{\frac{\alpha}{2}}$-error convergences for $\alpha = 1.2, 1.8, 2.2, 2.8$ are plotted in Figures 4 and 5. We observe a similar convergence behavior to the last example.

Example 4. In this test, we compare the accuracy of the Hermite–Galerkin method with the Hermite-collocation method. Letting $\rho \equiv 1$, we consider two cases: (i) $f(x) = e^{-x^2/2}(1 + x)$ and (ii) $f(\boldsymbol{x}) = e^{-x_1^2/2-x_2^2/2}(1 + x_1)(1 + x_2)$, and examine the maximum errors by the collocation and Galerkin methods for different α. The scaling parameter λ is fixed to be 0.4, and the numerical solution with $N = 512$ is used as reference solution.

From Figures 6–7, we observe that the Galerkin method leads to a higher accuracy than the collocation method. However, the Galerkin method is more expensive than the collocation method, particularly in the multidimensional case. We list the CPU time in Table 4 with the Galerkin and the collocation methods. For the Galerkin method, two different values of threshold $\epsilon = 10^{-8}$ and 10^{-12} are used. The table

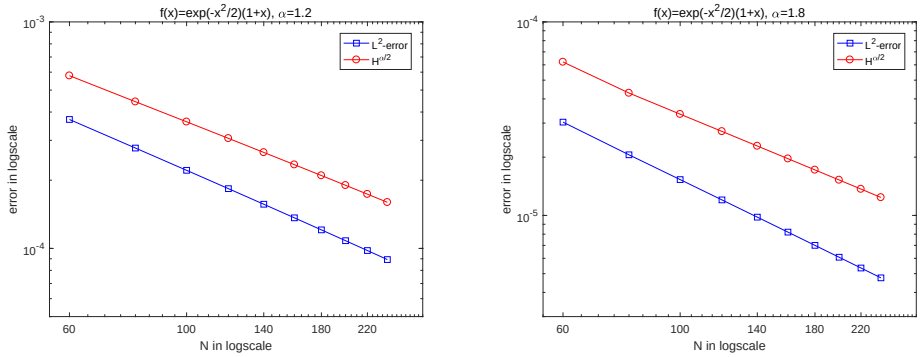

FIG. 3. *Convergence rates for* $f(x) = e^{-x^2/2}(1+x)$*; left:* $\alpha = 1.2$*, right:* $\alpha = 1.8$.

TABLE 2
Convergence rates of the L^2 *and* $H^{\frac{\alpha}{2}}$ *errors for* $f(x) = e^{-x^2/2}(1+x)$, $\alpha = 1.2$.

N	$L^2 - error$	Order	$H^{\frac{\alpha}{2}} - error$	Order
80	2.77e-004		4.44e-004	
100	2.21e-004	-1.01	3.62e-004	-0.92
120	1.84e-004	-1.02	3.06e-004	-0.92
140	1.57e-004	-1.03	2.65e-004	-0.93
160	1.36e-004	-1.03	2.34e-004	-0.93
180	1.21e-004	-1.04	2.10e-004	-0.94
200	1.08e-004	-1.04	1.90e-004	-0.94
220	9.79e-005	-1.05	1.74e-004	-0.95
240	8.93e-005	-1.06	1.60e-004	-0.95

TABLE 3
Convergence rates of the L^2 *and* $H^{\frac{\alpha}{2}}$ *errors for* $f(x) = e^{-x^2/2}(1+x)$, $\alpha = 1.8$.

N	$L^2 - error$	Order	$H^{\frac{\alpha}{2}} - error$	Order
80	2.06e-005		4.29e-005	
100	1.53e-005	-1.32	3.34e-005	-1.13
120	1.20e-005	-1.33	2.72e-005	-1.12
140	9.80e-006	-1.33	2.28e-005	-1.13
160	8.20e-006	-1.34	1.96e-005	-1.13
180	7.00e-006	-1.34	1.72e-005	-1.13
200	6.08e-006	-1.34	1.52e-005	-1.14
220	5.35e-006	-1.34	1.37e-005	-1.14
240	4.76e-006	-1.35	1.24e-005	-1.14

lists the total CPU time by solving the two-dimensional problem *10 times* and using Matlab 2016 on a Lenovo Thinkpad laptop with Intel Core i7-6600 CPU. We observe that the collocation method is much faster than the Galerkin method with the same number of unknowns, while the accuracy improvement of the Galerkin method is problem dependent. It appears that for most problems, the collocation method would be more efficient than the Galerkin method. However, for more general problems with variable coefficients, the efficiency of the collocation method will be lost.

5.2. Application to fractional advection-dispersion equation. We consider the following fractional advection-dispersion equation [4, 3, 16]:

$$\frac{\partial u(x,t)}{\partial t} + v\frac{\partial u(x,t)}{\partial x} + \mathcal{D}(-\triangle)^{\frac{\alpha}{2}}u(x,t) = 0,\ x \in \mathbb{R},\ t \in [0,T] \tag{5.1}$$

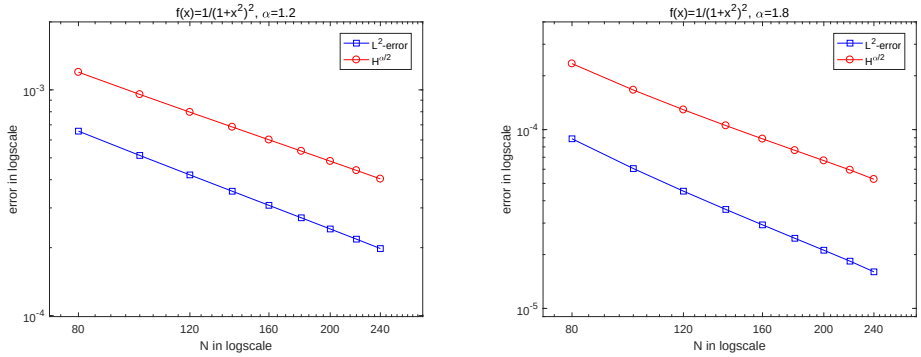

FIG. 4. *Convergence rates for* $f(x) = \frac{1}{(1+x^2)^2}$*; left:* $\alpha = 1.2$*, right:* $\alpha = 1.8$.

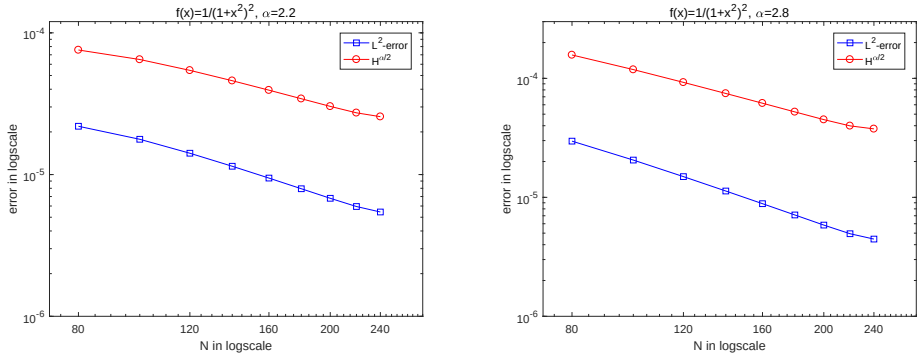

FIG. 5. *Convergence rates for* $f(x) = \frac{1}{(1+x^2)^2}$*; left:* $\alpha = 2.2$*, right:* $\alpha = 2.8$.

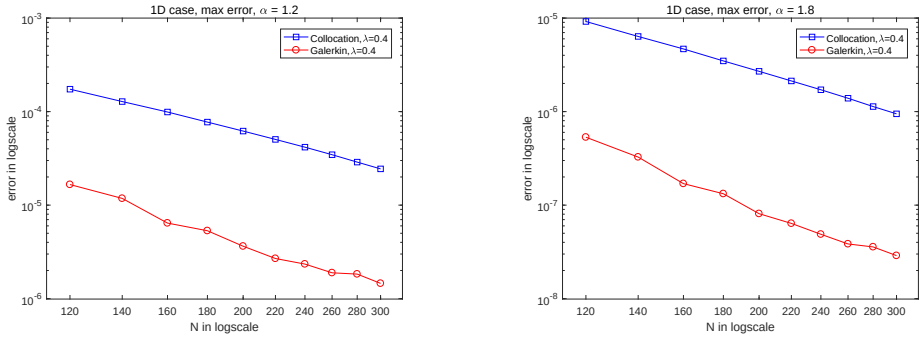

FIG. 6. *Maximum error with spectral collocation and spectral Galerkin method the one-dimensional case,* $f(x) = e^{-x^2/2}(1+x)$*; left:* $\alpha = 1.2$*, right:* $\alpha = 1.8$.

with the initial condition

$$u(x,0) = \delta(x), \tag{5.2}$$

where v is a given constant mean velocity, $\mathcal{D}$ is a diffusion coefficient, and $\delta(x)$ is the Dirac mass.

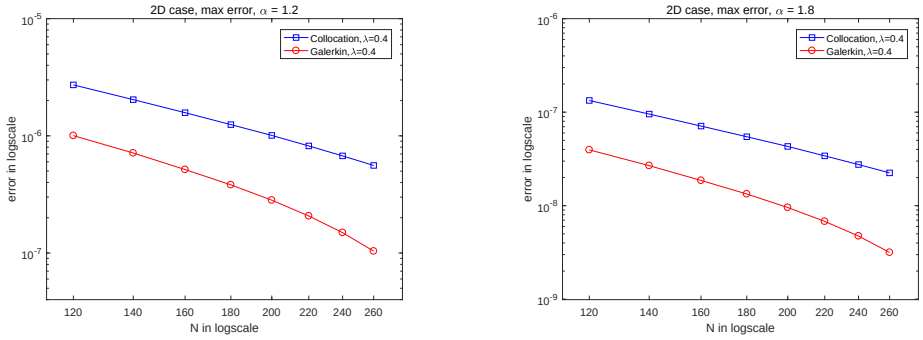

FIG. 7. *Maximum error with spectral collocation and spectral Galerkin method for the two-dimensional case,* $f(\boldsymbol{x}) = e^{-x_1^2/2-x_2^2/2}(1+x_1)(1+x_2)$*; left:* $\alpha = 1.2$*, right:* $\alpha = 1.8$.

TABLE 4

Total CPU time (in seconds) by solving the two-dimensional problem 10 *times with the Galerkin or collocation method (G—Galerkin, C—Collocation),* $\lambda = 0.4$.

	$\alpha = 1.2$			$\alpha = 1.8$		
N	G, $\epsilon = 10^{-8}$	G, $\epsilon = 10^{-12}$	C	G, $\epsilon = 10^{-8}$	G, $\epsilon = 10^{-12}$	C
200	5.08	7.02	0.241	3.94	5.13	0.225
300	23.1	31.0	0.663	17.8	23.5	0.660

Set

$$u_N(x,t) = \sum_{m=0}^{N} \tilde{u}_m(t)\psi_m(x), \tag{5.3}$$

$$U_N(t) = (\tilde{u}_0(t), \tilde{u}_1(t), \ldots, \tilde{u}_N(t))^T. \tag{5.4}$$

Apply the same procedure as we did before, and note that $\widehat{\delta}(\xi) = \frac{1}{\sqrt{2\pi}}$, then we have the semidiscretized system

$$\begin{aligned} \frac{d}{dt}U_N(t) + (vC + \mathcal{D}S)U_N(t) &= 0, \\ U_N(0) &= U_N^0, \end{aligned} \tag{5.5}$$

where S is given in (4.3) and

$$C = (c_{kj})_{k,j=0}^{N},\ c_{kj} = \int_{-\infty}^{\infty} \psi_j'(\xi)\psi_k(\xi)d\xi, \tag{5.6}$$

$$U_N^0 = (\tilde{u}_0^0, \tilde{u}_1^0, \ldots, \tilde{u}_N^0)^T,\ \tilde{u}_j^0 = \frac{\mathrm{i}^j}{\sqrt{2\pi}} \int_{-\infty}^{\infty} \psi_j(\xi)d\xi. \tag{5.7}$$

For the time discretization of (5.5), we use a second order backward Euler scheme, which is

$$\frac{3U_N^{n+1} - 4U_N^n + U_N^{n-1}}{2\Delta t} + (vC + \mathcal{D}S)U_N^{n+1} = 0,\ 1 \le n \le M-1, \tag{5.8}$$

where $\Delta t = \frac{T}{M}$ is the time step, U_N^n is the discretized vector solution of $U_N(t)$ at time $t = t_n = n\Delta t$. The backward Euler scheme was used to obtain U^1. It is clear that this scheme is unconditionally stable and the convergence rate is $O(\Delta t^2)$.

We first consider problem (5.1) without the advection term, i.e., $v = 0$. The other parameters are set as follow: $\mathcal{D} = 1$, degree of space approximation is $N = 200$, time step $\Delta t = 10^{-3}$. The solutions at time $T = 2$ for $\alpha = 1.2, 1.5, 1.8$ are plotted in Figure 8.

To study the asymptotic behavior of the fractional diffusion equation (5.1) ($v = 0$) when $|x| \to \infty$, we also plot in Figure 9 the numerical solution in interval $x \in [5, 11]$ in log-log scale at time $T = 2$. We observe that the solutions have algebraic decay for

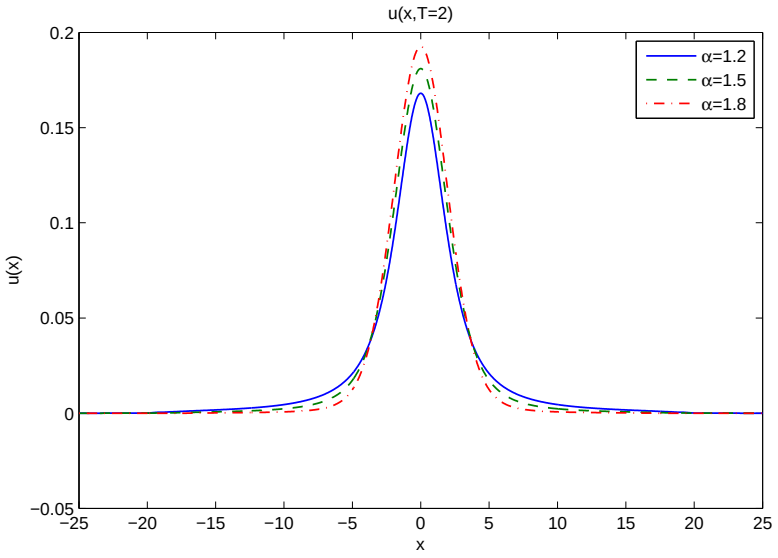

FIG. 8. *Solution $u(x,t)$ at time $T = 2$ for different values of α.*

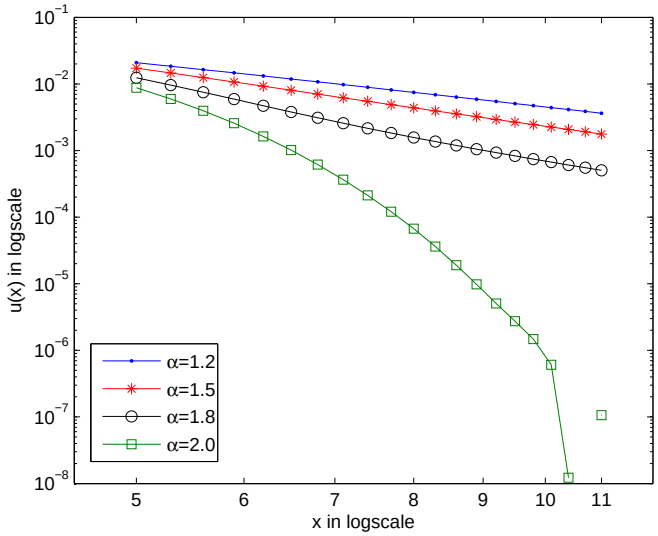

FIG. 9. *Numerical solution $u(x,t)$ on $x \in [5, 11]$ in log-log scale for different values of α, $T = 2$.*

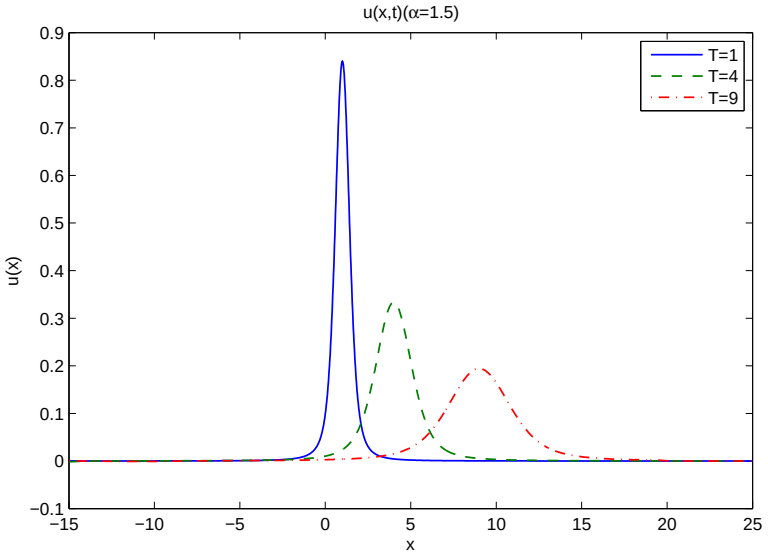

FIG. 10. *Solution $u(x,t)$ at different times with $\alpha = 1.5$.*

all values of α except in the case $\alpha = 2$ (standard diffusion) where the solution decays exponentially.

Next, we set $v = 1$ in (5.1). Other parameters are $\mathcal{D} = 0.2$, $N = 200$, time step $\Delta t = 10^{-3}$.

The solutions with $\alpha = 1.5$ at different times are plotted in Figure 10. As expected, the velocity $v = 1$ pushes the solution to the right.

5.3. Application to a fractional nonlinear Schrödinger equation. We consider the following two-dimensional fractional nonlinear Schrödinger equation (fNLS) [11]:

$$\begin{aligned} &\mathrm{i}\partial_t u(\boldsymbol{x},t) = \frac{1}{2}(-\triangle)^{\frac{\alpha}{2}} u(\boldsymbol{x},t) + \gamma|u|^{2p}u(\boldsymbol{x},t),\ \boldsymbol{x}\in\mathbb{R},\ t\in(0,T], \\ &u(\boldsymbol{x},0) = u_0(\boldsymbol{x}), \end{aligned} \tag{5.9}$$

where $\mathrm{i}^2 = -1$ and $p > 0$, $u(\boldsymbol{x},t)$ is a complex-valued wave function. Let $f(u) = \gamma|u|^{2p}u$, applying the Fourier transform on both sides of (5.9), we get

$$\begin{aligned} &\mathrm{i}\partial_t \widehat{u}(\boldsymbol{\xi},t) = \frac{1}{2}|\boldsymbol{\xi}|^{\alpha}\widehat{u}(\boldsymbol{\xi},t) + \widehat{f}(u)(\boldsymbol{\xi},t),\ \boldsymbol{\xi}\in\mathbb{R},\ t\in(0,T], \\ &\widehat{u}(\boldsymbol{\xi},0) = \widehat{u}_0(\boldsymbol{\xi}). \end{aligned} \tag{5.10}$$

In order to solve the above equation, we use the Hermite-collocation method for the space discretization and use a semi-implicit second order backward Euler method for time discretization. More precisely, the full discretization scheme in the phase space reads

$$\mathrm{i}\frac{3\widehat{u}_{kl}^{n+1} - 4\widehat{u}_{kl}^{n} + \widehat{u}_{kl}^{n-1}}{2\Delta t} = \frac{1}{2}|\boldsymbol{\xi}_{kl}|^{\alpha}\widehat{u}_{kl}^{n+1} + \widehat{f}_{kl}(u^n),\ k,l = 0,1,\ldots,N, \tag{5.11}$$

with

$$\widehat{u}_{kl}^{0} = \widehat{u}_0(\boldsymbol{\xi}_{kl}),\ k,l = 0,1,\ldots,N,$$

where $\Delta t = T/M$ is the time step, $\widehat{u}_{kl}^n, k, l = 0, 1, \ldots, N, n = 0, 1, \ldots, M$ represent the point values of $\widehat{u}(\boldsymbol{\xi}, t)$ at $\boldsymbol{\xi} = \boldsymbol{\xi}_{kl} := ((\xi_1)_k, (\xi_2)_l)$ and time level $t_n = n\Delta t$, $\widehat{f}_{kl}(u^n)$ represent the point values of $\widehat{f}(u^n)(\boldsymbol{\xi})$ at $\boldsymbol{\xi} = \boldsymbol{\xi}_{kl}$ and time level t_n. Again, $\widehat{u}_{kl}^1$ are computed with the backward Euler method.

Once we have $\widehat{u}_{kl}^n, k, l = 0, 1, \ldots, N$, we can obtain the values at the Hermite–Gauss collocation points with a Hermite–Gauss transform. At each time step, the nonlinear terms $\widehat{f}_{kl}(u^n)$ are computed with the usual pseudospectral approach.

We take the initial condition to be

$$u_0(\boldsymbol{x}) = \eta sech(x_1) sech(x_2), \tag{5.12}$$

where η is a positive constant, and focus on the quintic case, i.e., $p = 2$. The other parameters are set to be $\eta = 1.0,\ N = 200,\ \Delta t = 10^{-3},\ \lambda = 0.6$.

We first consider the defocusing case with $\gamma = 1$. The modulus squared of the numerical solution at times $T = 1$ and $T = 2$ for different values of fractional order $\alpha = 1.1, 1.6$ are given in Figures 11–12. We observe that the solution diffuses as expected.

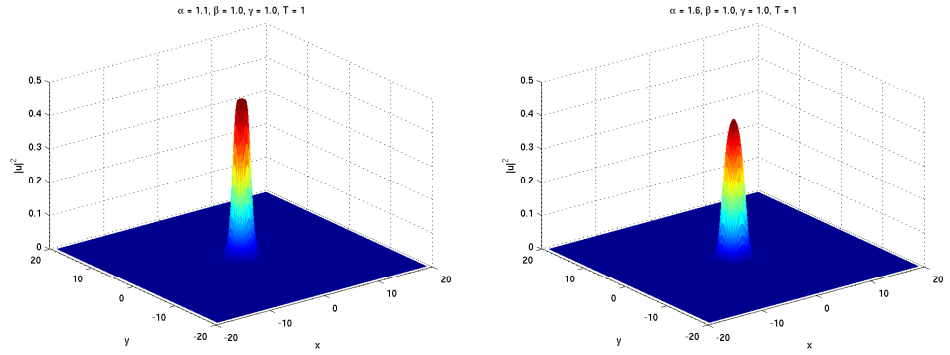

FIG. 11. *Defocusing case: modulus squared of the solution to the fNLS at time $T = 1$ with initial condition $sech(x_1)sech(x_2)$; left: $\alpha = 1.1$, right: $\alpha = 1.6$.*

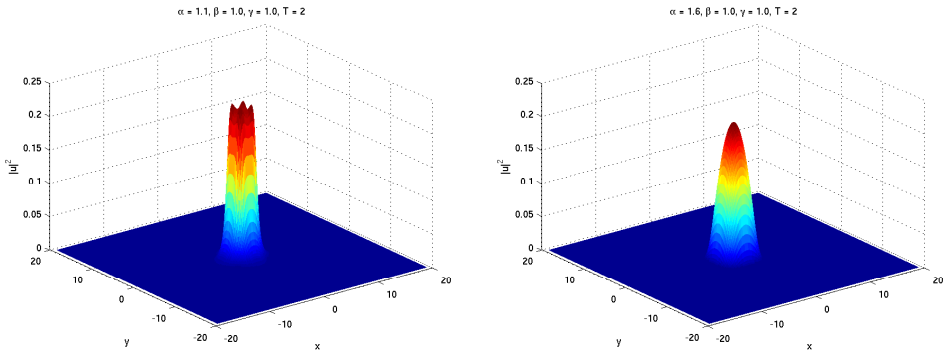

FIG. 12. *Modulus squared of the solution to the fNLS at time $T = 2$ with initial condition $sech(x_1)sech(x_2)$; left: $\alpha = 1.1$, right: $\alpha = 1.6$.*

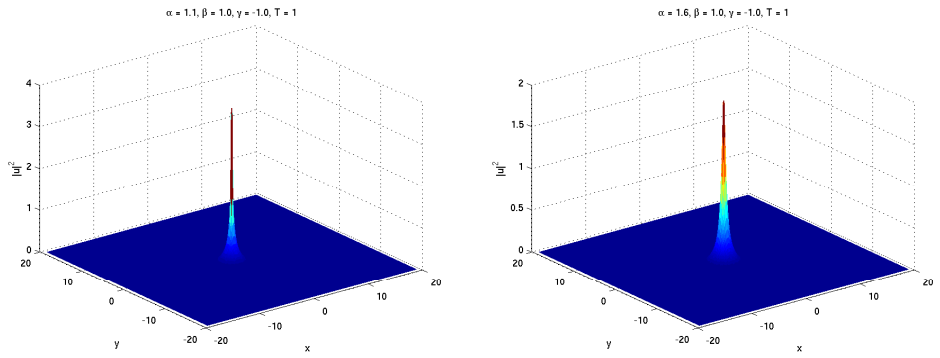

FIG. 13. *Focusing case: modulus squared of the solution to the fNLS at time* $T = 1$ *with initial condition* $sech(x_1)sech(x_2)$*; left:* $\alpha = 1.1$*, right:* $\alpha = 1.6$.

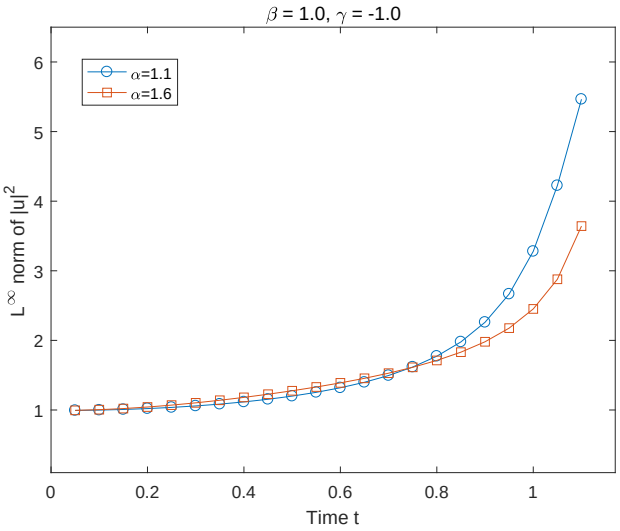

FIG. 14. *Evolution of the* L^∞ *norm of the modulus squared of the solution to the fNLS for the focusing case; initial condition* $sech(x_1)sech(x_2)$.

Next we consider the focusing case with $\gamma = -1$. In this case, the solution will eventually blow up. We plot the modulus squared of the numerical solution at time $T = 1$ for different values of fractional order $\alpha = 1.1$, 1.6 in Figure 13. The numerical results indicate that the maximum of the solution increases faster with smaller α, which is consistent with the observation in [11] where the one-dimensional fNLS is solved with up to $N = 2^{17}$ points using a Fourier spectral method. We also show the L^∞ norm of the modulus squared of the numerical solution in Figure 14. The modulus squared of the numerical solution quickly increases as time increases and eventually blows up.

6. Concluding remarks. Fractional diffusion equations are naturally derived on unbounded domains. Their solutions usually decay very slowly at infinity and it is not clear how to derive transparent boundary conditions at truncated boundaries. The

main purpose of this paper was to derive efficient spectral methods for fractional PDEs on unbounded domains directly to avoid errors introduced by domain truncations.

By using the key fact that Hermite functions are eigenfunctions of the Fourier transform, we developed efficient Hermite-collocation and Hermite–Galerkin methods for solving a class of fractional PDEs defined through Fourier transforms, and derived corresponding error estimates. In particular, the cost of our spectral methods for solving fractional PDEs on unbounded domains is of the same order as that for regular PDEs.

We applied these methods for solving fractional advection-diffusion equations and fNLS. The analysis and numerical results presented in this paper indicate that the proposed Hermite-collocation and Hermite–Galerkin methods are an effective approach to deal with fractional PDEs on unbounded domains directly.

REFERENCES

[1] R.A. Adams, *Sobolev Spaces*, Acadmic Press, New York, 1975.

[2] J. Aguirre and J. Rivas, *Hermite pseudospectral approximations. An error estimate*, J. Math. Anal. Appl., 304 (2005), pp. 189–197.

[3] D.A. Benson, R. Schumer, M.M. Meerschaert, and S.W. Wheatcraft, *Fractional dispersion, Lévy motion, and the made tracer tests*, in Dispersion in Heterogeneous Geological Formations, Springer, Dordrecht, Netherlands, 2002, pp. 211–240.

[4] D.A. Benson, S.W. Wheatcraft, and M.M. Meerschaert, *Application of a fractional advection-dispersion equation*, Water Res. Res., 36 (2000), pp. 1403–1412.

[5] J.P. Boyd, *Chebyshev and Fourier Spectral Methods*, Dover Mineola, NY, 2001.

[6] S. Chen, J. Shen, and L.-L. Wang, *Generalized Jacobi functions and their applications to fractional differential equations*, Math. Comp., 85 (2016), pp. 1603–1638.

[7] J. Duoandikoetxea, *Fourier Analysis*, Grad. Stud. Math. 29, American Mathematical Society, Providence, RI, 2001.

[8] W. Gautschi, *Orthogonal Polynomials: Computation and Approximation*, Numer. Math. Sci. Comput., Oxford University Press, New York, 2004.

[9] D.B. Haidvogel and T.A. Zang, *The accurate solution of Poisson's equation by expansion in Chebyshev polynomials*, J. Comput. Phys., 30 (1979), pp. 167–180.

[10] Y. He, P. Li, and J. Shen, *A new spectral method for numerical solution of the unbounded rough surface scattering problem*, J. Comput. Phys., 275 (2014), pp. 608–625.

[11] C. Klein, C. Sparber, and P. Markowich, *Numerical study of fractional nonlinear Schrödinger equations*, R. Soc. Lond. Proc. Ser. A Math. Phys. Eng. Sci., 470 (2014), 20140364.

[12] R.E. Lynch, J.R. Rice, and D.H. Thomas, *Direct solution of partial differential equations by tensor product methods*, Numer. Math., 6 (1964), pp. 185–199.

[13] Z. Mao, S. Chen, and J. Shen, *Efficient and accurate spectral method using generalized Jacobi functions for solving Riesz fractional differential equations*, Appl. Numer. Math., 106 (2016), pp. 165–181.

[14] P. Maroni and Z. da Rocha, *Connection coefficients between orthogonal polynomials and the canonical sequence: An approach based on symbolic computation*, Numer. Algorithms, 47 (2008), pp. 291–314.

[15] S.G. Samko, A.A. Kilbas, and O.I. Maričev, *Fractional Integrals and Derivatives*, Gordon and Breach, Philadelphia, 1993.

[16] R. Schumer, M.M. Meerschaert, and B. Baeumer, *Fractional advection-dispersion equations for modeling transport at the earth surface*, J. Geophys. Res. Earth Surf., 114 (2009), F00A07.

[17] J. Shen, T. Tang, and L.L. Wang, *Spectral Methods: Algorithms, Analysis and Applications*, Springer, Berlin, 2011.

[18] J. Shen, *Efficient spectral-Galerkin method* I. *Direct solvers for second- and fourth-order equations using Legendre polynomials*, SIAM J. Sci. Comput., 15 (1994), pp. 1489–1505.

[19] J. Shen and L.-L. Wang, *Some recent advances on spectral methods for unbounded domains*, Commun. Comput. Phys., 5 (2009), pp. 195–241.

[20] G. Strang, *Variational crimes in the finite element method*, in The Mathematical Foundations of the Finite Element Method with Applications to Partial Differential Equations, University of Maryland, Baltimore, MD, 1972, Academic Press, New York, 1972, pp. 689–710.

[21] T. Tang, *The Hermite spectral method for Gaussian-type functions*, SIAM J. Sci. Comput., 14 (1993), pp. 594–606.
[22] C.-L. Xu and B.-Y. Guo, *Hermite spectral and pseudospectral methods for nonlinear partial differential equations in multiple dimensions*, Comput. Appl. Math., 22 (2003), pp. 167–193.
[23] M. Zayernouri and G.E. Karniadakis, *Fractional Sturm-Liouville eigen-problems: Theory and numerical approximation*, J. Comput. Phys., 252 (2013), pp. 495–517.
[24] M. Zayernouri and G.E. Karniadakis, *Fractional spectral collocation method*, SIAM J. Sci. Comput., 36 (2014), pp. A40–A62.